nature astronomy

Supplementary information

https://doi.org/10.1038/s41550-024-02384-8

A core in a star-forming disc as evidence of inside-out growth in the early Universe

In the format provided by the authors and unedited

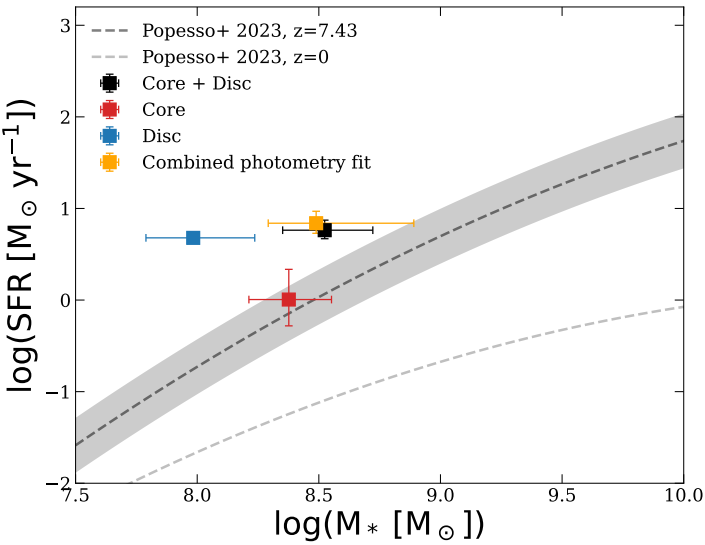

Supplementary Figure 1 Star-formation activity relative to the star-forming main sequence. The SFR (averaged over 10 Myr) against the stellar mass for the core, disc and combined components plotted in red, blue and black. The result of fitting the core+disc+clump photometry in also plotted in orange. The data is presented as the median of the distribution with the errors corresponding to the 16th and 84th percentiles. For reference, the star-forming main sequence (SFMS) [73] extrapolated to redshift 7.43 and at 0 is plotted as black and grey dashed lines, respectively (the shaded region corresponds to a 0.3 dex uncertainty region on the SFMS at $z = 7.43$). All components show elevated SFRs compared to the SFMS (by 0.6 and 1.2 dex for the core and disc, respectively).

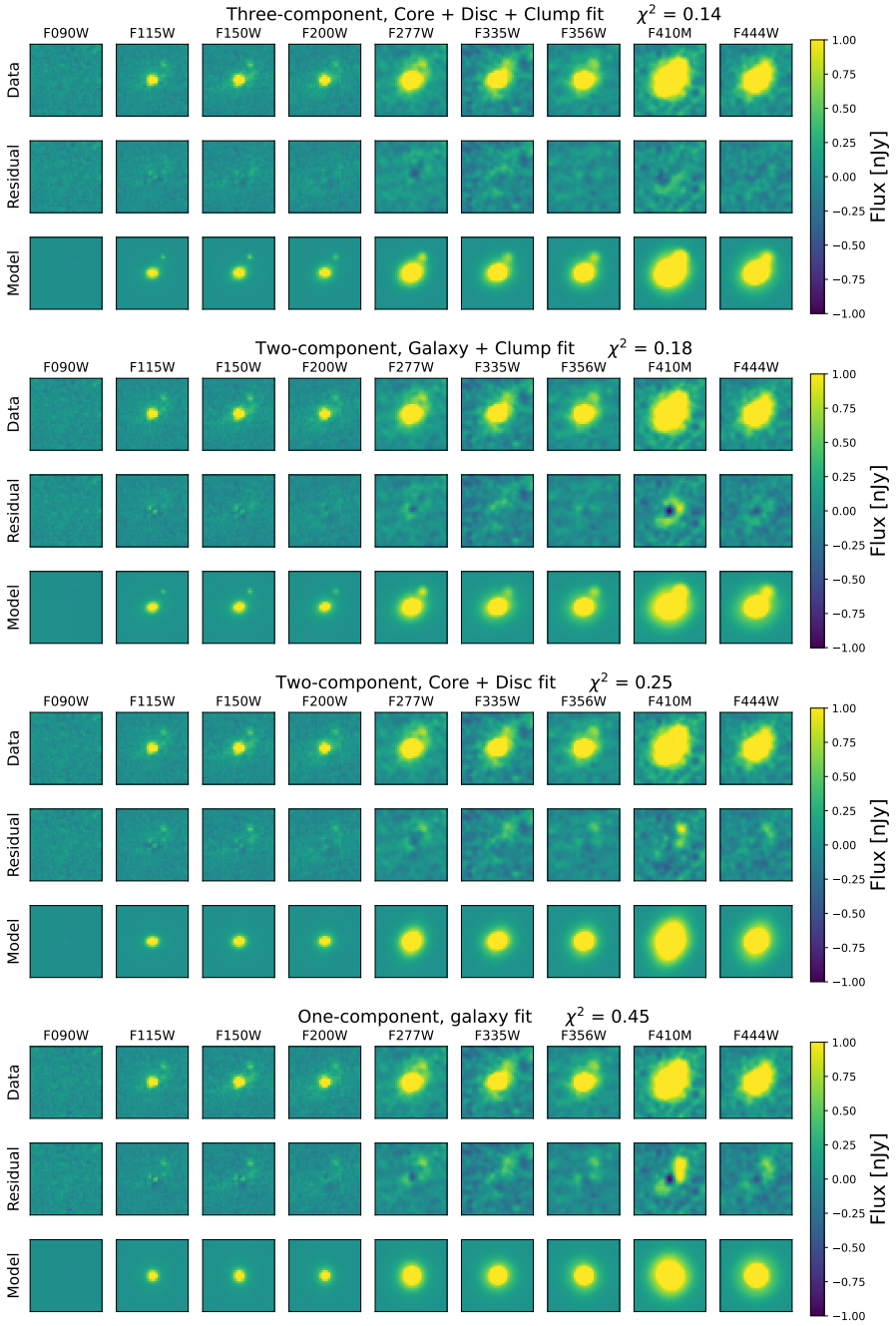

Supplementary Figure 2 Data, model, and residual maps for various ForcePho models. For each of the four main setups we plot the data, residual and model. The four setups are our fiducial, three-component fit (top panels), a two-component fit consisting of galaxy+clump (upper middle panels), a two-component fit consisting of a core+disc (with no clump),and a one-component single galaxy fit (bottom panels). It shows that the three-component fit appears to reproduce the data significantly better, as is quantified through the χ^2-value for the fit. This can also be seen in the residual figures for the other fits which all show more significant residuals (alongside their higher χ^2 values).

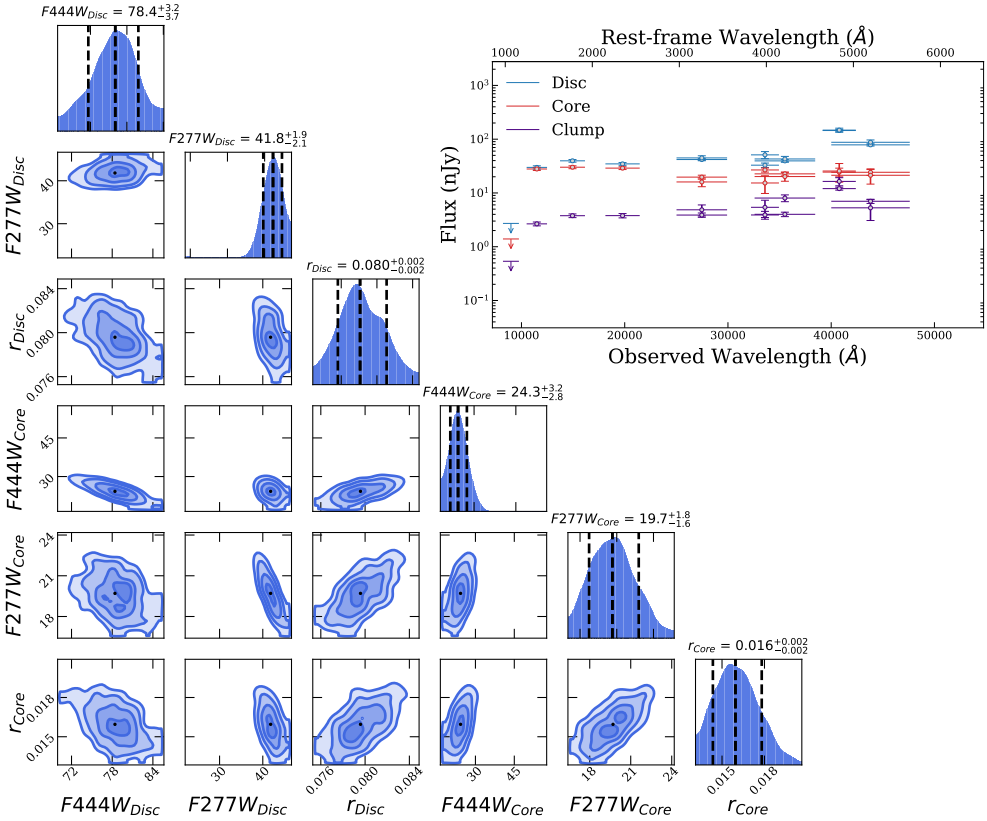

Supplementary Figure 3 Posterior distributions for the ForcePho fit and spectral energy distribution for the resulting components. Left panel: corner plot of the posterior distributions for flux in the F444W filter, F277W filter, and half-light radius for the disc and core component from the ForcePho fit. The corner plot shows that ForcePho constrains these parameters well. We find that the core and disc have a size of 16 ± 2 mas (82 pc) and 80 ± 2 mas (412 pc), respectively. We boost the errors of the core and disc to be a minimum of 20% in order to better account for systematics. Right panel: the spectral energy distribution (SED) of the core, disc and clump components. The x errors correspond to the filter widths, and the y errors correspond to the 1σ uncertainty propagated forwards from the error map.

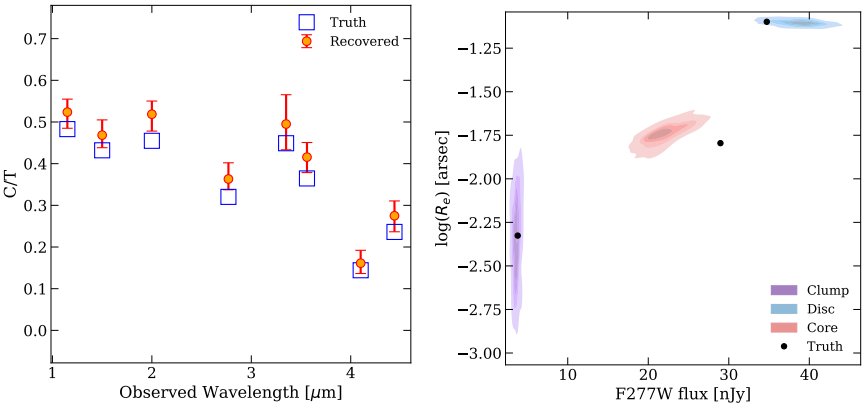

Supplementary Figure 4 Component recovery test with ForcePho. We simulate the best-fit 3-component model with Galsim, assuming the PSF from WebbPSF. We then refit this scene with ForcePho to determine the validity of ForcePho's PSF approximations. Left: the core-to-total (C/T) ratio from the original fit (truth) and the fit (recovered), plotted against filter wavelength. The data is presented as the median of the distribution with the errors corresponding to the 16th and 84th percentiles. Right: the half-light radius against flux in the F277W filter, the contours correspond to the posterior for the recovery tests, while the black point is the value from the original fit. These two plots show that ForcePho's PSF approximations are close to the true value and that we recover the fitted values close to the errors. The deviation seen in the contour plot is driven by the compact half-light radius of the core.

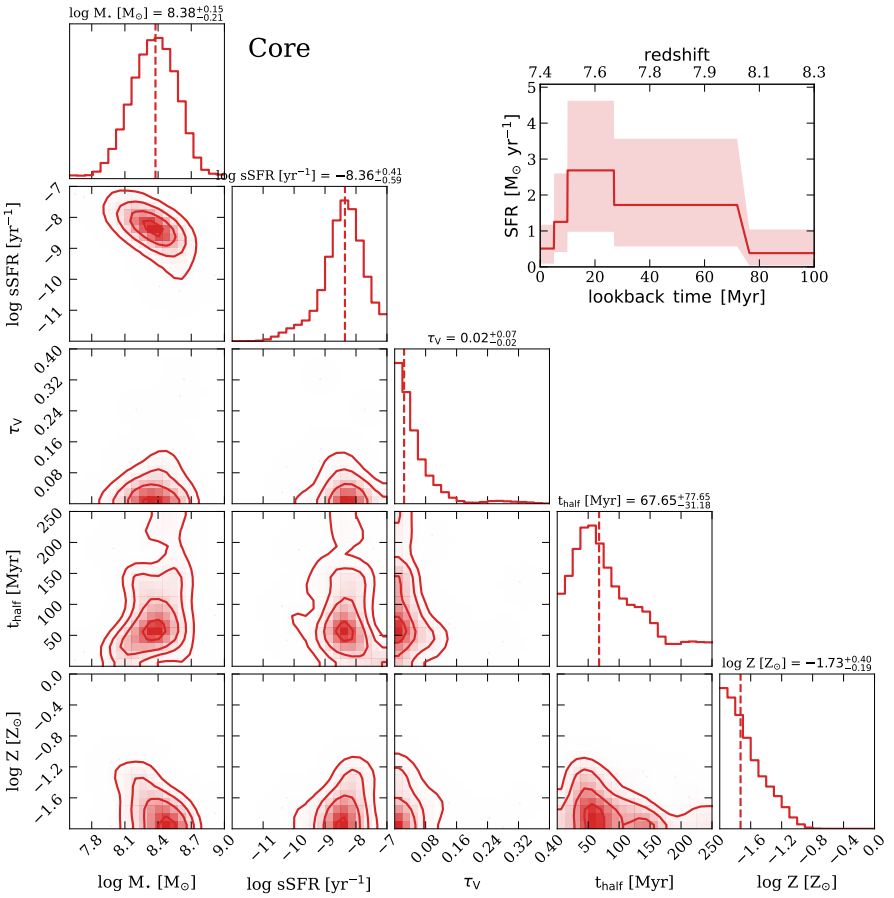

Supplementary Figure 5 Corner figure and star-formation history for the core component. Left: Corner plot showing stellar mass (M_*), specific star-formation rate (sSFR), optical depth (τ_ν), half-time ($t_{\rm half}$) and stellar metallicity (Z) for the core component as obtained by SED fitting. Right: the SFH for the core component. The data is presented as the median of the distribution with the errors corresponding to the 16th and 84th percentiles.

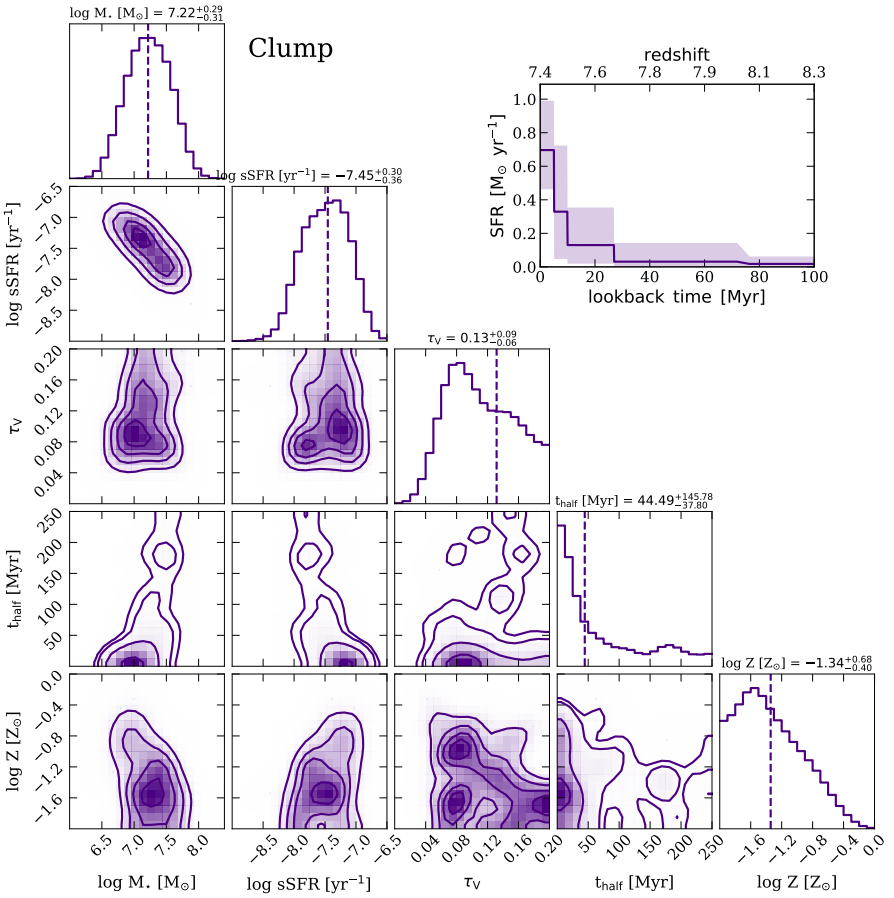

Supplementary Figure 6 Corner figure and star-formation history for the clump component. Left: Corner plot showing stellar mass (M_*), specific star-formation rate (sSFR), optical depth (τ_ν), half-time ($t_{\rm half}$) and stellar metallicity (Z) for the clump component as obtained by SED fitting. Right: the SFH for the clump component. The data is presented as the median of the distribution with the errors corresponding to the 16th and 84th percentiles.

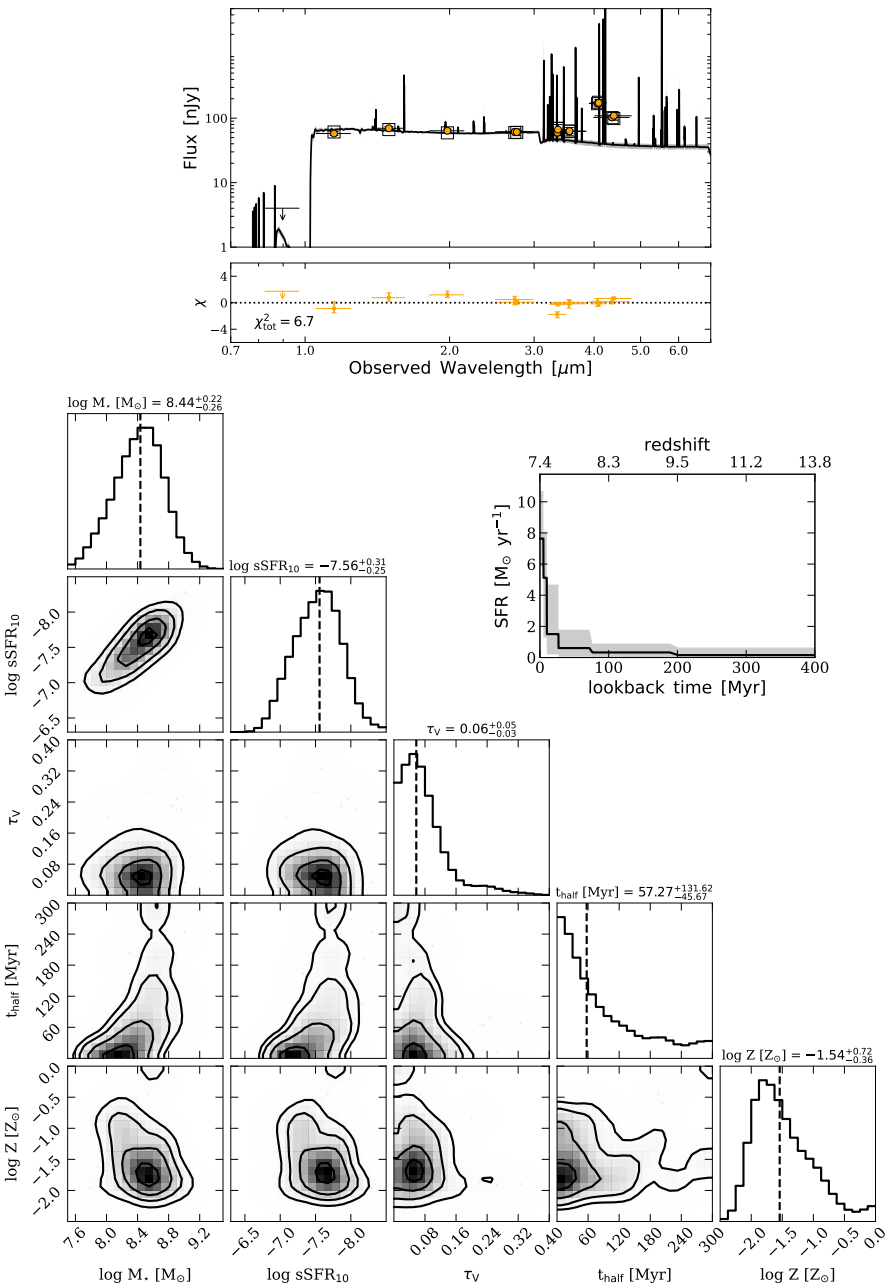

Supplementary Figure 7 SED fit, corner figure and SFH for the combined photometry. Upper panel: Spectral energy distribution (SED) fits for the single-component ForcePho fit. The yellow points show the photometry inferred from the ForcePho modelling, while the 2σ upper limits are indicated as downward pointing arrows. The errors correspond to the 1σ uncertainties from the photometric pipeline. The open squares mark the photometry from the best-fit SED model. The solid lines and the shaded regions show the median and the 16th-84th percentile of the SED posterior from the Prospector modelling, respectively. Lower panel: corner plot showing stellar mass (M_*), specific star-formation rate (sSFR), optical depth (τ_V), half-time (t_{half}) and stellar metallicity (Z) for the single component ForcePho fit as obtained by SED fitting, with the SFH inset. These two plots show that when fit as single component, the stellar mass and sSFR inferred, traces that of the combined galaxy.

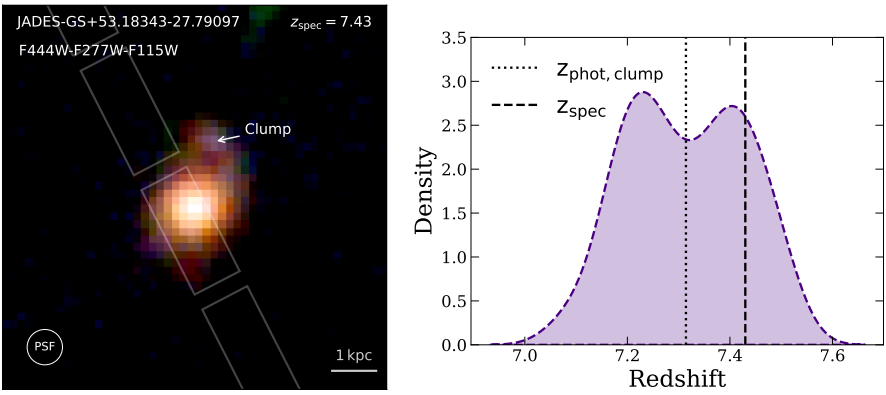

Supplementary Figure 8 RGB image highlighting the clump and 1D posterior distribution for the photometric redshift of the clump component. Left: RGB image of JADES-GS+53.18343-27.79097 with the clump position highlighted. Right: the marginalised posterior distribution for the photometric redshift of the clump component. We see it is double peaked but consistent with the spectroscopic redshift of the core and disc galaxy.

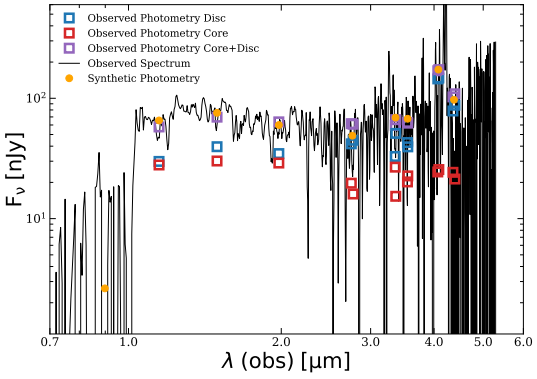

Supplementary Figure 9 The NIRSpec spectrum compared to the ForcePho photometry. The 1D NIRSpec spectrum (black) and synthetically derived photometry from the spectrum (orange points). The observed ForcePho photometry for the disc (blue), core (red) and combined core+disc galaxy (lilac) is overplotted. We find the synthetic photometry matches the photometry of the combined core + disc galaxy, highlighting that the combined medium- and broad-band photometry traces both the stellar continuum and nebular emission line.

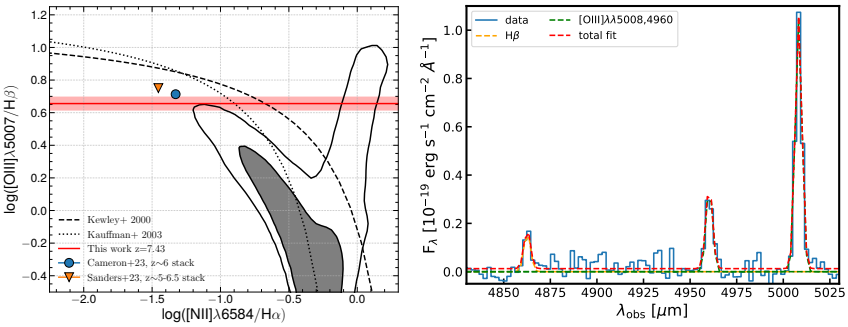

Supplementary Figure 10 Emission line diagnostic diagram and examination of fits to the R1000 spectrum. Left panel: A classical BPT [109] diagram showing the ratio of the emission lines [OIII]λ5007 to Hβ versus [NII]λ6584 / Hα. At this redshift NIRSpec can no longer detect [NII]λ6584 and Hα so we plot a red horizontal line for the value of [OIII]λ5007/Hβ, the colour fill corresponds to the 1σ error propagated through from the pipeline. We see that the galaxy is still consistent with a star-forming galaxy and shows similar [OIII]λ5007/Hβ ratios to other star-forming galaxies at these ratios [69]. Right panel: fits to the Hβ emission line and the [OIII] doublet. We see that both can be with standard Gaussians and that there is no need for an underlying broad component.